Environmental Earth Sciences (2023) 82:386
https://doi.org/10.1007/s12665-023-11058-z

ORIGINAL ARTICLE

Pathfinder elements and indicator minerals of Au from the Kubi Gold ore deposits in Ghana

Gabriel K. Nzulu[1] · Hans Högberg[1] · Per Eklund[1] · Lars Hultman[1] · Prosper M. Nude[2] · Abu Yaya[3] · Martin Magnuson[1]

Received: 17 January 2023 / Accepted: 15 July 2023 / Published online: 2 August 2023

Abstract

The Au mineralization in the Kubi Gold Mining Area in the Birimian of Ghana is associated with garnet (about 85 vol.%), magnetite, pyrrhotite, arsenopyrite, and sulfide minerals, as well as quartz with gold and calcite. These minerals and the included elements can act as indicator minerals or pathfinder elements. For the present work, we collected samples from drill holes at different depths, from the alluvial zone (0–45 m) to the ore zone (75–100 m). The distributions of minerals and elements in the rocks that act as indicator minerals and pathfinder elements in the concession area were investigated along the drill hole cross sections. X-ray diffraction shows that the samples contain garnet, pyrite, periclase, and quartz as the main indicator minerals. By energy-dispersive X-ray spectroscopy, Fe, Mg, Al, S, O, Mn, Na, Cu, Si, and K are identified as corresponding pathfinder elements. The results indicate that the Au mineralization in the Kubi Mine area correlates mostly with the occurrence of garnet, pyrite, goethite, and kaolinite in the host rocks, which show towards the surface increasingly hematitic and limonitic alteration in form of Fe(oxy-)hydroxides.

Keywords Pathfinder elements · X-ray · Spectroscopy · Birimian · Gold

Introduction

Au mineralization in the Kubi mining area (denoted the "513 zone") was discovered in 2010 during geochemistry (auger drilling, soil, and stream sampling), geophysics, geology, and diamond core drill exploration activities as part of extended exploration programmes over several decades (Smith and Amaor 2014). The findings suggest that within the Kubi area, the highest gold concentrations occur in deformed garnet-hornfelses that are part of the carbonaceous schist. The rocks contain a maximum of about 15 vol.% sulfide minerals comprising pyrite, pyrrhotite, and some arsenopyrite.

Elemental and mineral distributions in geological settings are important tools for identifying gold and other precious metals. In mineral exploration, indicator minerals that are resistant to weathering usually remain in the parent material. Examples of such minerals include zircon, apatite, quartz, titanite, rutile magnetite, chromite, ilmenite, and garnet of gemstone quality. Indicator minerals can also be found in till, soil, and stream sediments and are usually involved in specific mineralization, alteration, and can possibly be used for rock identification (McClenaghan 2005). The weakest resistant minerals to weathering, such as talc (McClenaghan 2005) and most rock salts (halites), are easily eroded or transported from one place to another. Pathfinder elements of gold include As, Mo, Ag, Sn, Sb, Te, W, Bi, Ni, and Cu (Bayari et al. 2019; Plouffe 2001; Somarin et al. 2021). The elements Sb, Nb, Ta, and Sn are often found in Au-bearing minerals or pegmatite rocks and can easily be distinguished from their rutile mineral signatures (Porter et al. 2020).

Previously, studies on pathfinder elements and indicator minerals in Ghana have mainly involved statistical methods with a multivariate numerical approach to identify trace elements such as Fe, Mn, Ag, As, Cu, Zn, Ni, and Pb

✉ Gabriel K. Nzulu
gabriel.nzulu@liu.se

[1] Department of Physics, Chemistry and Biology (IFM), Linköping University, 58183 Dunkwa Municipal, Sweden

[2] Department of Earth Science, School of Physical and Mathematical Sciences, College of Basic and Applied Sciences, University of Ghana, P.O. Box LG 25, Legon-Accra, Ghana

[3] Department of Materials Science and Engineering, School of Engineering Sciences, CBAS University of Ghana, P.O. Box LG 25, 233 Legon-Accra, Ghana

associated with Au (Nude et al. 2012). As for progression, Bayari et al. (2019) applied X-ray diffraction (XRD) and inductively coupled plasma mass spectrometry (ICP-MS) to identify pathfinder elements and their indicator minerals in the Bole-Nangoli gold belt in the north-eastern part of Ghana. Recently, Nzulu et al. (2021a) applied X-ray photoelectron spectroscopy and energy dispersive X-ray spectrometry (EDX) to identify the pathfinder elements Ag, Hg and Ti that act as pathfinder elements in the host minerals of Au ore in the alluvial regime collected at a small-scale mining site at Kubi. These elements were attributed to the indicator minerals quartz, hematite, pyrite (marcasite), garnet, and other occasional silicate minerals, such as biotite and hornblende. Recent studies have focused on understanding the pathfinders of Au mineralisation in the western margin of the Ashanti Belt, the characterisation of Au indicator minerals (Nzulu et al. 2021a), and the elucidation of the pathfinder elements (Nzulu et al. 2021b) in the Kubi concession. As previous samples were collected in rather shallow deposits, at depths of 0–20 m in an artisanal mine, the above conditions call for further investigations to greater depths of ~ 100 m in the same concession area.

Materials and methods

Regional geology of Ghana

The southwestern part of Ghana is underlain by the Paleoproterozoic Birimian Supergroup, comprising thick sequences of northeasterly–southwesterly trending belts of steeply dipping metavolcanic rocks that alternate with metasedimentary rock units (Kesse 1985). The metavolcanic rocks consist of metamorphosed, basic, and intermediate lavas and pyroclastic rocks, and the metasedimentary rocks comprise phyllites, schist, and greywackes (Leube et al. 1986). Both the metavolcanic and the metasedimentary units have been intruded by syn- and post-tectonic granitoids (Kesse and Foster 1984). There are two types of granitoids: the basin granitoids, which intrude the metasedimentary basins, and the belt granitoids, which are usually restricted to the volcanic and volcano-sedimentary assemblages. The Tarkwaian group, which represents erosional deposits of earlier lithologies (Leube et al. 1986; Kesse and Foster 1984) occupies the troughs within the Birimian in Ghana. All the major gold deposits in Ghana are hosted by Birimian and Tarkwaian rocks and are usually associated with shearing and granite intrusions, mostly along the margins of metavolcanic and metasedimentary rocks.

Description of the Kubi concession

The Kubi deposit lies in a rippling and topographically low zone with a weathering profile between 15 and 20 m thick. The boundaries are defined by a series of 'pillar points' in longitude and latitude coordinates with a unique Ghana datum referred to as the Legion 1929 Datum. The Kubi pillar points are registered with the Minerals Commission of Ghana as follows P1 (6° 01′ 54″ 6° 01′ 54″), P2 (5° 59′ 39″ 1° 43′ 12″), P3 (5° 58′ 12″ 1° 44′ 18″), P4 (5° 58′ 16″ 1° 45′ 57″), P5 (5° 59′ 21″ 1° 45′ 11″), P6 (5° 59′ 21″ 1° 45′ 11″), P7 (6° 01′ 19″ 1° 44′ 28″), P8 (6° 01′ 14″ 1° 44′ 02″), and P9 (6° 01′ 54″ 1° 43′ 17). The mineralization profile of Au, which is dominated by saprolite, increases into the transition and ferruginous clay zone, mainly consisting of minerals of garnet, goethite, and kaolinite that are heavily altered by hematite and limonite (Smith and Amaor 2014). Samples from the diamond drill core show that native Au is associated with garnet and the sulphide group of minerals and is disseminated within conglomerates, quartz felsite, phyllites, and gabbroic rocks as shown in Fig. 1. Historically, and even to date, numerous alluvial artisanal small-scale mining activities occurred in several localities within the Proterozoic unit of the Ashanti belt, which received the most gold-rush attention along the Offin river.

Sample collection and preparation

The samples were collected from a drill hole with identification number KV10-522 (Fig. 1) with an azimuth of 290° and a dip of − 60° at three different depths: namely, the saprolite zone (0.0–43.5 m), moderately–slightly weathered (59.0–78.85 m), and slightly weathered Au rich zone (78.85–100 m). The saprolite sample contains quartz fragments, of which most are anhedral–euhedral to rounded pebbles and cobbles, as shown in Fig. 2a. A piece of pyrite was taken from a moderately weathered zone in Fig. 2b, anda half-core sample from the garnet zone was crushed into smaller fragments in Fig. 2c. The dried samples were not subjected to any form of pre-treatment to chemically remove carbonates, iron oxides, silt, clay, organic matter, and other impurities. Prior to XRD, SEM, and EDX measurements, these samples were tested with acid, and the reactions showed weak (in the pyrite sample) to strong (in the quartz and garnet–gabbro samples) neutralization reactions with carbonate ($CaCO_3$).

From the top surface down to ~ 10 m, lateritic, clay, conglomerates, and silt profiles are found containing roots, stones, and decayed materials debris. The highly saprolite

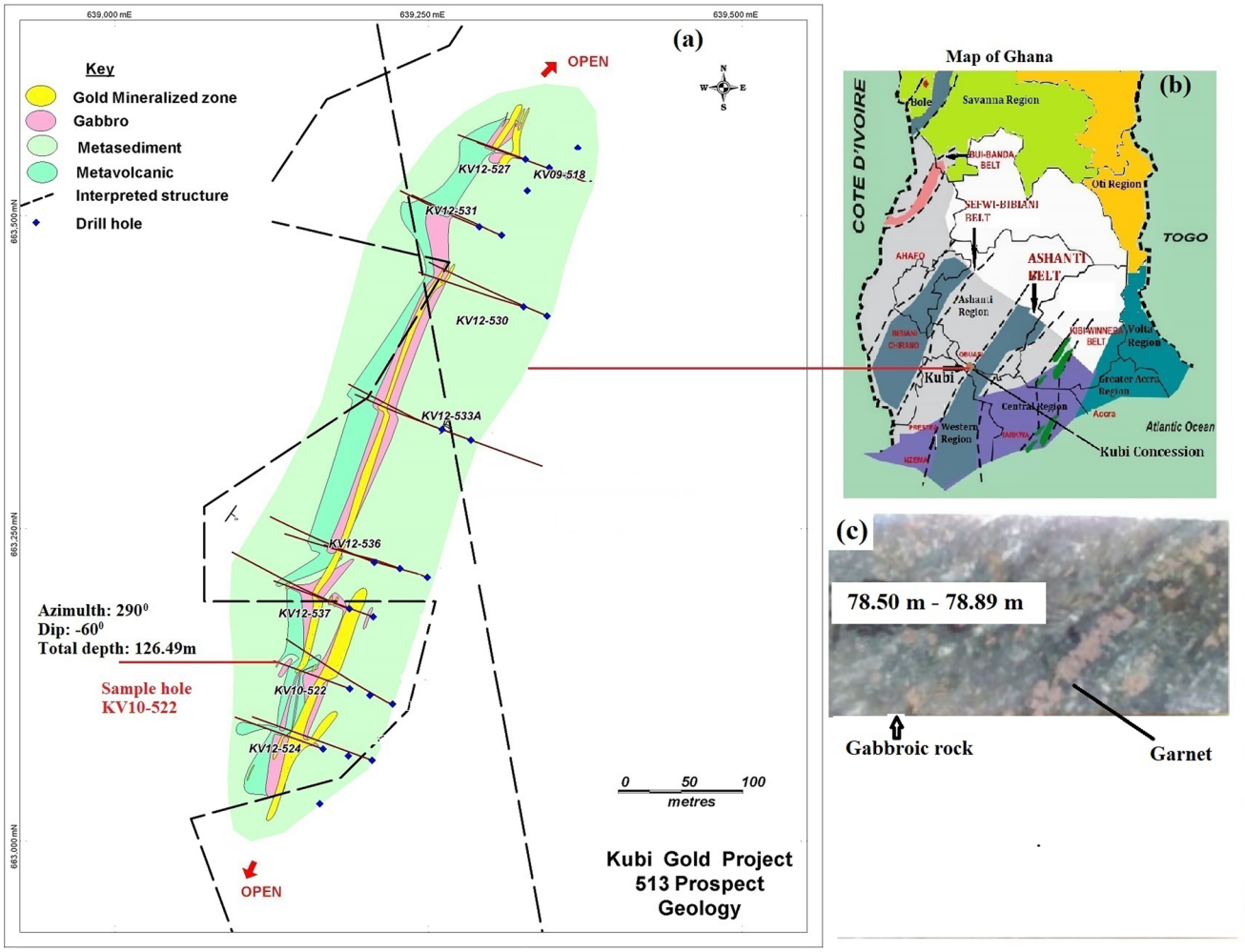

Fig. 1 Map of Kubi pit showing drill holes cutting across the Au mineralization zone (513 prospects) **b** part of the map of Ghana showing Kubi concession **c** half core gabbroic rock with garnet mineral. [Maps generated by G. K. Nzulu, Fred Akosah, and Douglas MacQuarrie from MapInfo software]

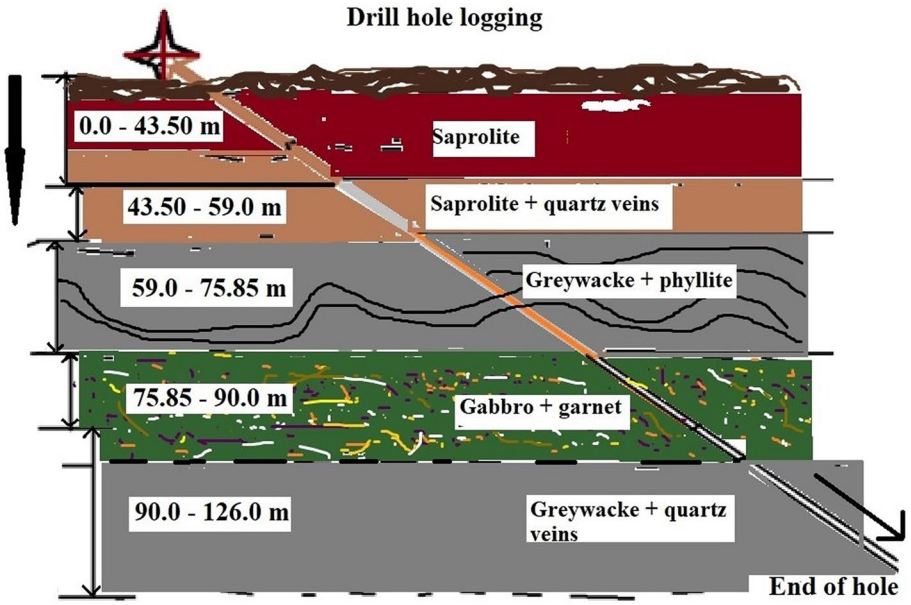

Fig. 2 Drill hole showing geological logging and sampling depth of KV10-522 (Kubi village, the year 2010, and drill hole number 522) **a** quartz samples [0.0–43.5 m], **b** pyrite, [59.0–75.85 m] and **c** garnet–gabbro samples [75.85–100.0] m from the Kubi mining concession

profile, stretching in length to about ~ 43.5 m, contains quartz pebbles in gravel- and cobble-bearing weathered material, and hosted by hematite-, limonite-, and chlorite-bearing material, with sections of graphitic to phyllitic alteration. Moderately weathered graywacke with weak carbonate alterations, Fe stains, and spotty pyrites continues the drill profile to ~ 59 m.

Between ~ 59 m and ~ 78.85 m, a bedded, moderate–slightly weathered greywacke with occasional phyllitic sections contains pyrite, pyrrhotite, chalcopyrite, and spotty garnet.

A slightly weathered to fresh garnet-rich gabbro (garnet zone) underlies the greywake to a depth of 100 m. In it occur gold, pyrite, pyrrhotite, chalcopyrite, arsenopyrite, and carbonates. Under the garnet zone an alternating sequence of gabbro, greywacke is intersected to the end of the drill hole in about 126 m depth. Smaller portions of felsite, basalt, and quartz veins, containing pyrite veining, carbonates, and occasional garnet, can be found included.

Measurements

Figure 2 shows the images of (a) quartz, (b) pyrite, and (c) garnet–gabbro samples from the Kubi mining concession area. Qualitative and semiquantitative analysis (XRD and EDX) were applied to characterize the Au-bearing host rocks, including the mineral chemistry of minerals associated with the Au mineralization at different depths at the concession site.

XRD analyses were performed on a PANAnalyical X'pert powder diffractometer with a θ–2θ configuration using a Cu-Kα radiation wavelength of 1.5406 Å (45 kV and 40 mA) with a scan step size of 0.0082°, counting time of 19.68 s per step, and a scan range of 10° and 100° in 2θ scans. During the measurement, the samples were constantly rotated on a spinner stage. The XRD data were quantitatively analyzed using Rietveld refinement with the aid of the MAUD (Marquardt 1963) software, where analytical functions were used for the modeling. The background parameters were refined simultaneously with the lattice parameters, peak shape, crystal structure, microstructure, strain, and texture in the refinement while considering the least squares for the iteration (Marquardt 1963; Lutterotti 2010).

The samples were also analyzed using a Zeiss Supra 35 VP field emission SEM operated at 20–30 kV. This SEM is equipped with an EDX detector, which is used for elemental mapping to investigate the elemental distribution of the samples. The samples were prepared by fitting the crystalline solid samples into aluminum stubs with the aid of carbon sticky tabs.

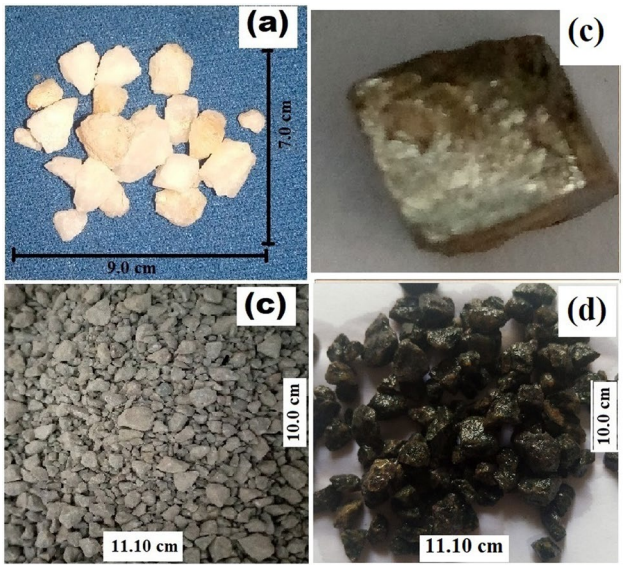

Fig. 3 Images of **a** quartz, **b** pyrite, **c** dry garnet–gabbro, and **d** wet garnet–gabbro samples from the Kubi mining concession area

Results

XRD results

Figure 3a–c shows XRD patterns of quartz, pyrite, and almandine-type garnet from gabbroic rock. The diffractogram of quartz in Fig. 3a shows pronounced peaks of high-intensity reflections from pure quartz (PDF No. 00-033-0664) (Lignie et al. 2012). The XRD pattern of the pyrite in Fig. 3b reveals the presence of pure pyrite according to (PDF No. 00-033-0664) in agreement with the literature (Bayliss 1977). In the case of almandine-type garnet–gabbro in Fig. 3c, the low-intensity reflections correspond to almandine-type garnet (PDF No. 000-89-4373) and periclase (MgO), consistent with the literature (Armbruster et al. 1992; Hazen 1976). The high-intensity reflections reveal the presence of quartz and biotite (PDF No. 00-002-0057) due to their dominance in the parent rock material and in accordance with the literature (Lignie et al. 2012; Brigatti et al. 2000). Most results correspond to the logging codes in Table 1 and the assay results in Table 2.

The XRD Rietveld refinement details obtained for the selected minerals: quartz, pyrite, and garnet in gabbro from Fig. 3 are listed in Table 3. A few weak additional peaks reveal the existence of additional mineral phases containing biotite and periclase. The unit cell parameters of all identified minerals are listed in Table 3 and are in good agreement with reference data (Lignie et al. 2012; Bayliss 1977; Armbruster et al. 1992; Hazen 1976; Brigatti et al. 2000; Geiger et al. 1992).

Table 1 Logging codes assigned to different lithology, mineralogy, alteration, veining types, and structures, relevant to the present study

Lithology		Mineralogy		Alteration		Veining		Structure	
Code	Description	Code	Description	Code	Description	Code	Description	Code	Description
LAT	Laterite	PYRT	Pyrite	OXDZ	Oxidized	QZVN	Quartz veining	FALT	Fault/fault zone
SAP	Saprolite	PYRH	Pyrrhotite	HMTT	Hematite	PYVN	Pyrite veining	SHZN	Shear/shear zone
GWKE	Greywacke	ASPY	Arsenopyrite	LMTT	Limonite			BEDD	Bedding
ARG	Argillite	GOLD	Gold	CLAY	Clay			MASS	Massive
GR	Granite	HMTT	Hematite	CHL	Chlorite			VN	Vein
FS	Felsite	LMTT	Limonite	CAL	Calcite				
VLCC	Volcano clastic	CLAY	Clay	CARB	Carbonate				
PHYL	Phyllite	CHL	Chlorite	GRAPH	Graphite				
QTZT	Quartzite	CAL	Calcite						
TRANS	Transition	CARB	Carbonate						
QZVN	Quartz veining	CHPY	Chalcopyrite						
PYVN	Pyrite veining	GARN	Garnet						
QZCARB	Quartz > Carbonate veining								
Ga	Gabbro								

Table 2 Assay results of diamond drill hole No. KV10-522

Kubi drilling BH NO: KV10-522 LINE NO: 39.5N AZM: 290° DIP: − 60							Sample description
Sample no	From (m)	To (m)	Length (m)	Wt (g)	Au avg	Lith code	
KV 522-001	75.40	75.90	0.50	1.160	0.53	GWPH	Greywacke and Phyllite; foliated + qtz stringers
KV 522-002	75.90	76.50	0.60	1560	0.84	Ga	**Gabbro**, coarse grained + large red garnets + py (2%)
KV 522-003	76.50	77.00	0.50	2361	0.65	Ga	**Gabbro**, coarse grained + large red garnets + py (3%)
KV 522-004	77.00	77.85	0.85	2765	0.36	Ga	**Gabbro**, coarse grained + large and small red garnets + py (1–2%)
KV 522-005	77.85	78.50	0.65	1720	0.21	Ga	**Gabbro**, coarse grained + occas very small red garnets + py (1–2%)
KV 522-007	78.50	79.00	0.50	3449	0.04	Ga	**Gabbro**, coarse grained, no red garnets; occas py bleb
KV 522-022	92.00	93.00	1.00	2586	0.48	Ga	**Gabbro**, med grained + scattered qtz stringers
KV 522-026	96.00	97.00	1.00	2295	0.53	Ga	**Gabbro**, med − fine grained
KV522-028	98.00	99.00	1.00	1980	**3.02**	Ga	**Gabbro**, med − fine grained + scattered qtz veinlets
KV 522-042	110.00	111.00	1.00	1900	0.41	Ga	**Gabbro**, med − fine grained + qtz veins
KV 522-045	113.00	114.00	1.00	1120	0.95	Ga	**Gabbro**, vuggy, fine grained + vuggy qtz veins
KV 522-047	115.00	116.00	1.00	2156	0.81	Ga	**Gabbro**, med − fine grained + qtz veinlets and stringers
KV 522-048	116.00	117.00	1.00	1580	**1.40**	Ga	**Gabbro**, vuggy, med − fine grained + 15 cm QV, partly vuggy
KV 522-049	117.00	118.00	1.00	820	**1.20**	Ga	**Gabbro**, vuggy, fine grained + 10 cm QV
KV 522-251	119.00	119.60	0.60	1260	**1.41**	Ga	**Gabbro**, fine grained + qtz stringers
KV 522-052	119.60	120.05	0.45	860	0.03	Fel	Felsite, v fine grained, buff colour, sheared, slightly foliated
KV522-054	121.20	122.00	0.80	1380	0.04	PH	Phyllite, sheared + qtz boudins and veins
KV 522-055	122.00	122.70	0.70	840	0.12	Mn	Mn, sheared, dark purple–brown + qtz veins
KV 522-061	126.00	126.49	0.39	600	0.03	Bas	Basalt, very fine grained, greenish, + py specks

Geochemical analysis of the mineralized zone 75–120 m in ppm as shown in Fig. 4a

Bold indiates the high grade Au content and the rock containing the gold

Table 1 lists the mineral codes used for geological logging in this mining area shown in Fig. 4. Table 2 shows the assay results of the drill hole samples of the mineralized zone (75–120 m). The results from the geochemical analysis show an Au range of 0.5–3.02 ppm containing indicator minerals such as pyrite, quartz veins, and garnet in the

Table 3 Rietveld refinement details obtained for quartz, pyrite, almandine, periclase, and biotite

Parameter	Quartz	Pyrite	Almandine	Periclase	Biotite
Molecular formula	SiO_2	FeS_2	$Fe_3Al_2Si_3O_{12}$	MgO	$AlFHKMg_2O_{12}\ Si_3$
$a=b=c$ (Å)	4.91, $c=5.41$	5.41	11.52	4.21	5.344, 9.256, 10.237
$\alpha=\beta=\gamma$ (°)	90, $\gamma=120$	90	90	90	90, 100.27, 90
V (Å^3)	113.02	159	1530.8	74.512	498.251
Z	3	4	8	4	2
Space group	P3221	Pa-3	Ia-3d	Fm-3m	C12/m1
ρ (g/cm^3)	2.65	5.01	4.05	3.78	2.80
R_{wp} (%)	24.02	17.06	22.4	19.18	18.34
R (%)	15.6	11.48	13.64	12.62	13.14
R_{exp} (%)	9.8	6.24	7.40	4.86	8.04

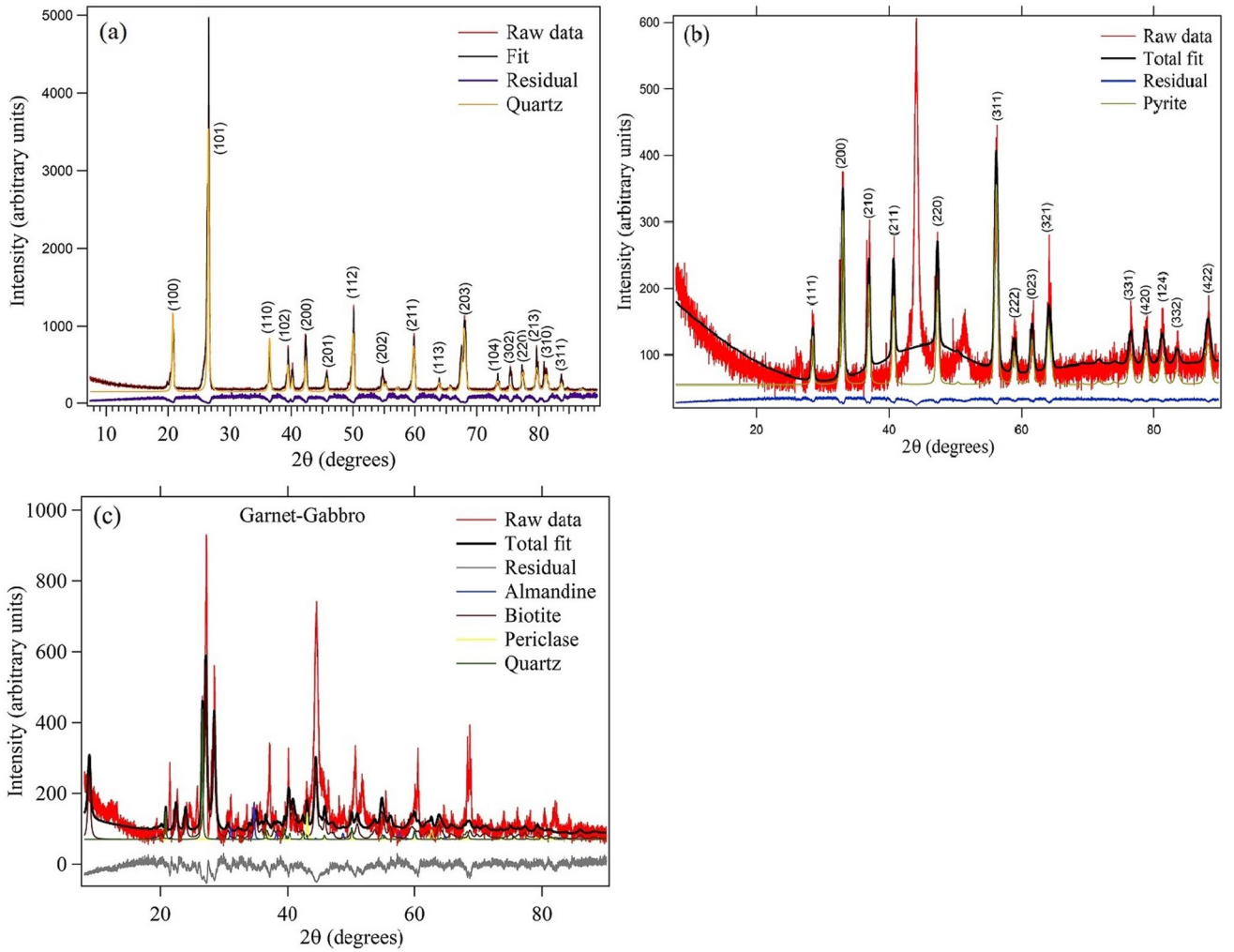

Fig. 4 XRD pattern of **a** quartz, **b** pyrite, and **c** almandine-type garnet [in gabbro] samples in the present work

gabbroic rocks. The higher Au values of 1.50 and 3.02 can be attributed to strong carbonatic, graphitic, or phyllitic alterations.

In the XRD analysis, only the identifiable minerals with well-pronounced peaks could be refined and quantified. Since the Au is contained in speckles of garnet mineral

within the gabbroic rocks (Kesse and Foster 1984), and from the Kubi geological core logging manual in Table 1, the refinement was focused on garnet peaks. Gabbroic rocks containing plagioclase and pyroxene with minor hornblende, olivine, and accessory minerals are not configured in the refinement process, since they are not part of the pathfinder mineralization of Au in the study area but are rather part of the rock-forming minerals of gabbro. The refinement model used in the fitting of the almandine-type garnet took into consideration the atomic coordinates for oxygen within the three crystallographic axes, while all other elements were fixed at their respective positions.

SEM/EDX results

Figure 5 and Table 4 show an EDX analysis of the mass ratios of the elemental components associated with quartz, pyrite, and almandine-type garnet used for mineral identification. The EDX spectra of these minerals (Fig. 5) reveal

Table 4 Elements identified in the analysis of EDX for quartz, pyrite, and almandine type garnet samples

Elemental	Quartz (at.%)	Pyrite (at.%)	Garnet (at.%)
Fe	–	27	12
S	–	52	0
Si	21	–	2
O	58	–	58
C	18	21	21
Al	–	–	1
Mn	–	–	2
K	1	–	0
Cl	1	–	0
Ca	–	–	4
Na	1	–	–
Total	100	100	100

With the 0.01 detection limits of the EDX, the atomic percentages are normalized to their nearest percentage units

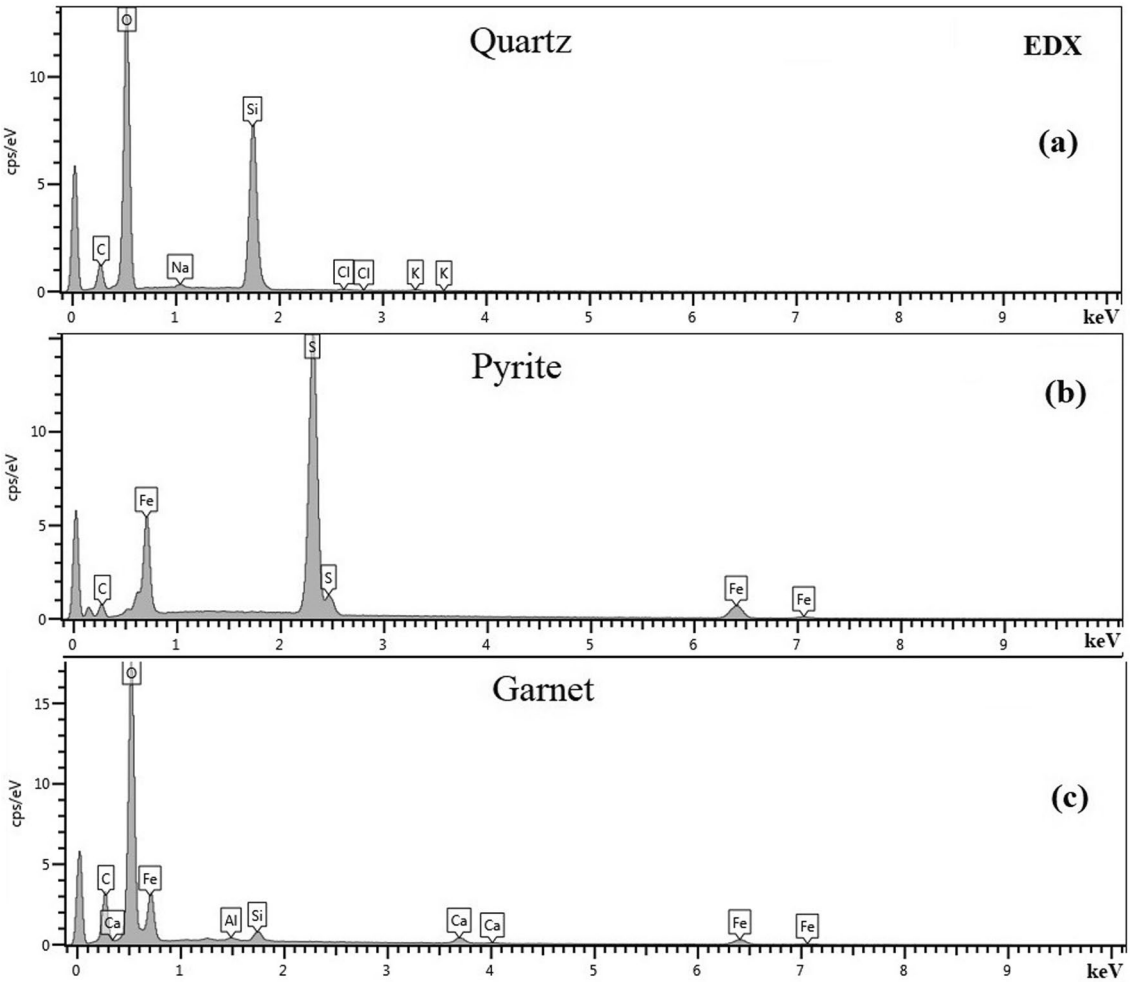

Fig. 5 EDX spectra showing elemental distribution for the **a** quartz, **b** pyrite, and **c** almandine-type garnet parts of the gabbro sample

that the quartz sample part consists mainly of Si, O, and C with minor components of K, Cl, and Na; pyrite consists of Fe and S; and almandine consists of Fe, Al, Si, O, and Ca, with a minor amount of Mn, consistent with the assay results of Table 2.

Figure 5a–c shows the EDX spectra of quartz, pyrite, and almandine-type garnet. In Fig. 5a, the quartz spectra consist of Si and O as the main elemental components, with C, Na, K, and Cl as impurity species, likely due to the segregation of C and the incorporation or surface contamination of Na, K, and Cl in SiO_2 (Götte et al. 2011; Ali et al. 2019). As revealed by the EDX of pyrite in Fig. 5b, the Fe, S, and C indicate that the sample mainly contains FeS_2. The elemental components of the data in Fig. 5c of Fe, Si, O, C, Al, Ca, and Mn indicate the presence of nesosilicate antiferromagnetic minerals of the garnet type: $Fe^{2+}{}_3Al_2Si_3O_{12}$ (almandine) (Geiger et al. 1992) in addition to the impurity-related elements Ca and Mn. The presence of carbon as revealed by the EDX data could be attributed to adventitious carbon, graphite, or carbonates that serve as potential mineral alterations in the concession, according to Table 1.

Table 4 gives quantitative EDX results for the assigned peaks corresponding to quartz, pyrite, and garnet in each sample obtained at different focal spots on the samples. The weakly distributed elemental components with characteristic peaks in the EDX spectra suggest the presence of impurity phases that may act as pathfinder elements. These can be assigned to their respective indicator minerals per Table 1. The EDX could not detect the presence of Au in the randomly selected grains, which may not contain spots of speckled garnet from the crushed garnet–gabbro fragments or be below the detection limit for Au at − 0.1 at.%.

Figure 6a–c shows SEM images of quartz, pyrite, and almandine-type garnet from the samples under investigation. The morphology of the quartz in Fig. 6a shows mussel–shell-like surfaces with a few spots of apparent flat, angular to conchoidal fracture with spots of crystal overgrowth. Without considering mechanical features caused by the drilling, the image indicates that the textures of the quartz surface depend on the particular geological setting in the Kubi area, the transportation process, and the depositional environment (Nzulu et al. 2021a, b; Kesse 1985). This unweathered material has spotty alterations of weak carbonates. In the case of the pyrite sample in Fig. 6b, spotty grains of quartz mineral and internal fractures or irregular cracks are identified with alterations of graphite and carbonates. The almandine-type garnet in the gabbroic material in Fig. 6c shows dodecahedral shapes and casts

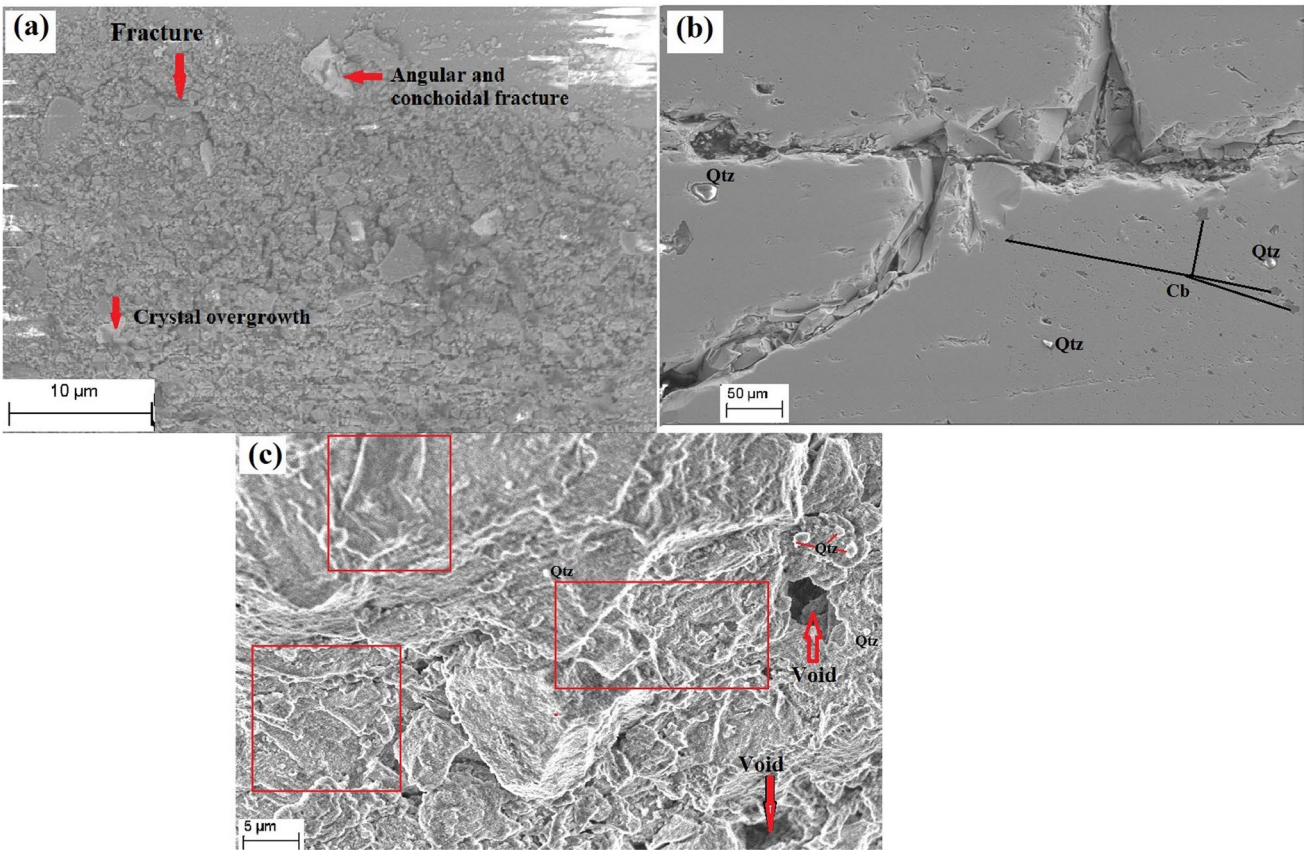

Fig. 6 SEM image morphology of **a** quartz, **b** pyrite, and **c** almandine-type garnet in gabbro

of euhedral and undulating pit shapes. These voids, fractures/cracks are indicative of weaker zones of highly rich-mineralized material representing the Kubi orebody that is also moderately strongly altered by carbonates.

Discussion

The identified minerals from the XRD are consistent with the mineralogy/lithological logging codes, EDX elemental distributions are attributed to alteration/mineralogical codes, and the SEM findings are assigned to structural/geotechnical logging codes in agreement with Table 1 and the assay result in Table 2. The elemental distributions for EDX in Table 4 that show Si, O, K, Cl, and Na for quartz; Fe and S for pyrite; and Fe, Si, O, Al, Mn, and Ca for garnet indicate the presence of these minerals as Au indicators as well as other impurities (Lignie et al. 2012; Bayliss 1977; Hazen 1976; Brigatti et al. 2000; Götte et al. 2011; Ali et al. 2019). These elements are products/components of the minerals identified in the analysis: that is garnet–[Mg, Fe, Mn]$_3$Al$_2$(SiO4)$_3$, pyrite–FeS$_2$, goethite–Fe$_3^+$O(OH), arsenopyrite–(FeAsS), and quartz-SiO$_2$. The Na, K. Mn could be from the feldspars in the host rocks.

These results agree with the geochemical analysis of Table 2 that shows stringers–vuggy quartz, pyrite, and garnets in gabbro rocks and occasional phyllite and greywacke. The presence of C in all the samples is attributed to graphitic or carbonate alterations (Dochartaigh et al. 2011). The SEM image of the garnet in gabbroic rock in Fig. 6c shows some occurrences of surface layer euhedral shapes consistent with expectations for garnet that show a variety of fractured textures and shapes containing quartz, periclase, and biotite. The periclase is believed to have originated from the gabbroic rock, which mainly consists of olivine. Olivine can undergo a reversible reaction to form a mixture of perovskite and ferropericlase (Lin et al. 2007) according to the equation $\gamma-(\mathrm{Mg,Fe})_2\left[\mathrm{SiO_4}\right] \leftrightarrow (\mathrm{Mg,Fe})\left[\mathrm{SiO_3}\right]+(\mathrm{Mg,Fe})\mathrm{O}$ within the transition zone. Therefore, the periclase in the garnet–gabbro sample is a confirmation of a breakdown of olivine mineral within the hydrothermal formation of the rock/mineral assemblage.

The periclase (MgO) in the garnet gabbroic rock can undergo a chemical reaction and break up the oxide. This increases the amount of Mg elements in the mineral assemblage, and the Fe component can be replaced by the dominant Mg under certain conditions of temperature, pressure, and pH that promote the mineral to transform into pyrope-rich garnet ($Mg_3Al_2(SiO_4)_3$) (Geiger et al. 1992). Although the XRD refinement excludes the pyrope-type garnet as a component in the sample, it explains why the breakup reaction of MgO has not occurred. Periclase (MgO) causes hematite mineral alteration of magnesium hydroxide in most hydrothermal vein rocks in the Kubi area as well as in the soil sediments. Apart from performing a vital role in the ferruginous–garnet–hematite enrichment, the hematite alteration mineral derived from periclase also acts as a useful source of nutrients for the Kubi soils, balancing the soil acidity and pH level.

As shown in the cross section of the drill hole of the Kubi concession in Fig. 1, the garnet minerals containing periclase in the orebody at > 75 m below the soil surface, alter into hematite and protrude from greater depths through the transition zone (59–75 m depth) and finally into the oxide zone (0–59 m) to form the rich alluvial Au ore deposit found in the Kubi saprolite. It can be anticipated that during the chemical weathering and transport process, the almandine garnet can undergo a weathering process to cause a mineralogical change and transform into hematite. Hematite transforms into goethite under a hydration process (Graham et al. 1989a, b), since the Fe molar volume in goethite is greater than that of hematite (Campbell and Schwertmann 1984). Therefore, the dominant hematite alterations in the Kubi concession are associated with garnet–periclase-rich indicator minerals. Thus, the ferrous iron end member of the garnet mineral class represents an important silicate group of rock-forming minerals that constitutes the main component of the Kubi terrain and the rock transition zone (Geiger et al. 1992). The results indicate that the almandine-type-garnet can be considered as part of the main indicator minerals in Table 1 apart from the pyrite, arsenopyrite, chalcopyrite, and carbonates that are known to geologists in the concession area. These mineral compositions that trend down the soil can be ascribed to the presence of plutonic or orogenic activities considering the types of metasediments and metavolcanic terrain rocks such as amphibolite, hornblende gneiss, biotite gneiss, quartzite, iron formation, metaconglomerate, marble, pelitic schist, etc. (Kesse and Foster 1984) that form part of the Birimian–Tarkwaian supergroup (Kesse 1985).

The natural quartz fragments show the extent to which the sediments have been transported in high-energy subaqueous environments (Helland and Holmes 1997); predominantly by the Offin and Gyimi rivers, and their weathering profile due to the spotty flat–angular–conchoidal fracture and crystal overgrowth nature of the material. Therefore, we anticipate that the mineralogy of this surface terrain has an impact on the chemical weathering reaction of garnet (almandine), such that different products of indicator minerals occur in fractions within sediments from the top to the orebody. Thus, the disseminated minerals (periclase, biotite, pyrite, other sulfates, and oxides) are influenced by the flow mechanism of garnet and other indicator minerals depending on the density, mineralogy of by-products, and environmental conditions (Price et al. 2013), such that the reaction

mechanism of the weathering products of garnet within the study area depends on the composition of almandine experiencing weathering profiling.

From the results, we attribute the identified elements as constituents of the indicator minerals as well as pathfinder elements of Au mineralization. The identified elements Fe, Ag, Al, N, Ca, and Mn, K, Cl, O, Si, and Ti form either alloys with gold or with innate elements in the soil sediments and can be ascribed to primary geochemical distribution from the crystallization of magma and hydrothermal fluids (Nzulu et al. 2021b). Some of these identified elements, such as Si and Ag, are strongly associated with Au due to their eutectic characteristics, while N, C, and O have affinity for S or are associated with sulfide minerals. In addition, the migration of metasomatic elements and the rapid rate of chemical weathering of minerals from garnet zone lateralization in secondary processes might be contributing factors in the alteration and mineral distribution in the area.

There are four major gold deposits in the Ashanti belt, of which Kubi forms a part. The steeply dipping quartz veins in shear zones in the Birimian sedimentary rocks show mesothermal deposits, where Au mineralization occurs at moderate temperature and pressure along openings or fractures in rocks from hydrothermal fluids at intermediate depths. Thus, the hydrothermal fluids from the orebody at the Kubi concession deposit gold along openings of quartz and other silicate groups of minerals. The sulfide ores pyrite and arsenopyrite that are closely associated with quartz veins, gold, rounded pebbles, and cobbles in the Kubi concession are formed by auriferous deposits. This type of deposit usually results from the solidification of molten magma to form igneous rocks such as the gabbroic rock in the Kubi concession area, which contains the host Au garnet and periclase minerals. In addition, in the Ashanti belt, there are deposits associated with sulfide disseminations and stockworks in granitoids, where the sulfide is destroyed at pressure oxidation and the gold is converted into metallic form as free or visible gold in the rocks. These stockworks veins consist of quartz, calcite, pyrite, and arsenopyrite, which are important indicator minerals in the Kubi concession. Finally, the gold that occasionally occurs, particularly within conglomerates and in a smaller amount within the interbedded quartzite, reveals a palaeoplacer gold mineralization of the Tarkwaian Group caused by hydrothermal alterations that deposit the gold as free gold in the milieu of the conglomerates and as inclusions in other mineral grains. From Table 2, the Au assay result shows that the Au grades downward, indicating that these hydrothermal activities resulted in a low-grade distribution of gold mineralization horizons in the Kubi concession above the garnet zone.

We anticipate that the indicator minerals at the Kubi concession area, from the oxide zone to greater depths (the ore zone), have experienced similar physical, chemical, and geological conditions and protruded from a hydrothermal system, where the minerals have been precipitated by hot fluids and altered by veins of surrounding rocks.

Conclusions

X-ray diffraction, scanning electron microscopy, and energy dispersive X-ray spectroscopy were applied for identifying and comparing pathfinder elements and indicator minerals at different depths in the Kubi mining area in Ghana. With these combined analytical techniques, we identified pathfinder elements and indicator minerals of Au in a diamond drill hole; especially, the secondary mineral phases periclase and hematite that are present in the almandine-type garnet found in the gabbroic rock located at the mining area. Pathfinding elements Fe, Si, O, C, Al, Ca, Mg, Na, Mn, Cl, S, and K in the samples act as the main contributions to the indicator minerals; pyrite, quartz, periclase, and almandine-type garnet. Grains within sediments in the surface oxides are controlled by quartz and hematite, the bedrock contains pyrite and pyrrhotite, and the orebody contains garnet, periclase, and biotite as pathfinder minerals within the garnet zone. The analysis also indicates a mineralized oxide zone attributed to the orebody of several sulfide minerals and the segregation of alteration from garnet–periclase minerals to hematite. We attribute these indicator minerals to the four major types of primary Au mineralization that form part of the Ashanti belt: (1) sulfide mineral disseminations and stockworks in granitoids; (2) mesothermal, which comprises steeply dipping quartz veins in shear zones in Birimian sedimentary rocks; (3) sulfide ores containing auriferous arsenopyrite and pyrite that are closely associated with the quartz veins; and (4) paleoplacer deposits of the Tarkwaian Group, where gold occurs as free gold in the conglomerates. We conclude that the mineralogy of the alluvial zone is the chemical weathering reaction of almandine-type-garnet mineral from the orebody. This weathering process produces by-products such as periclase and hematite that act as pathfinders in the Kubi concession area.

Acknowledgements The authors thank the Swedish Government Strategic Research Area in Materials Science on Functional Materials at Linköping University (Faculty Grant SFO-Mat-LiU no. 2009 00971). M.M. acknowledges financial support from Swedish Energy Research (Grant no. 43606-1) and the Carl Tryggers Foundation (CTS20:272, CTS16:303, CTS14:310).

Author contributions GKN: Conceptualization, data curation, formal analysis, investigation, methodology, resources, software, validation, visualization, writing—original draft, and writing—review

and editing. HH: Supervision, project administration, validation, and writing—review and editing. PE: Supervision, project administration, validation, visualization, and writing—review and editing. LH: Funding acquisition, project administration, validation, and writing—review and editing. PMN: Validation, and writing—review and editing. AY: Validation, and writing—review and editing.

Funding Open access funding provided by Linköping University. The authors have not disclosed any funding.

Data availability Data will be available on request.

Declarations

Conflict of interest The authors declare no competing interests.

References

Ali AM, Padmanabhan E, Mijinyawa A (2019) Effect of pH on the stability of quartz in a multi-phase system of kaolinite, hydrous Al (hydr)oxide and quartz. SN Appl Sci 1:388

Armbruster T, Geiger CA, Lager GA (1992) Single-crystal X-ray structure study of synthetic pyrope almandine garnets at 100 and 293 K Py0-Alm100 at T = 293 K, Pyrope - Almandine join. Am Mineral 77:512–521

Bayari EE, Foli SK, Gawu Y (2019) The glacial transport and physical partitioning of mercury and gold in till: implications for mineral exploration with examples from central British Columbia, Canada. Environ Earth Sci 78:268

Bayliss P (1977) Am Mineral 62:1168

Brigatti MF, Frigieri P, Ghezzo C, Poppi L (2000) Crystal chemistry of Al-rich biotites coexisting with muscovites in peraluminous granites. Am Mineral 85:436

Campbell A, Schwertmann U (1984) Iron oxide mineralogy of placic horizons. J Soil Sci 35:569

Dochartaigh BÉÓ, Smedley PL, MacDonald AM, Darling WG, Homoncik S (2011) Groundwater chemistry of the carboniferous sedimentary aquifers of the Midland Valley; British Geological Survey, groundwater program: Scotland, UK

Geiger C, Armbruster T, Lager G, Jiang K, Lottermoser W, Amthauer G (1992) A combined temperature dependent 57Fe Mössbauer and single crystal X-ray diffraction study of synthetic almandine: evidence for the Gol'danskii-Karyagin effect. Phys Chem Min 19(2):121–126

Götte T, Pettke T, Ramseyer K, Koch-Müller M, Mullis J (2011) Cathodoluminescence properties and trace element signature of hydrothermal quartz: a fingerprint of growth dynamics. Am Mineral 96:802

Graham R, Weed S, Bowen L, Buol S (1989a) Weathering of iron-bearing minerals in soils and saprolite on the North Carolina blue ridge front: I. Sand-size primary minerals. Clays Clays Miner 37:19

Graham R, Weed S, Bowen L, Buol S (1989) Weathering of iron-bearing minerals in soils and saprolite of the North Carolina Blue Ridge Front: II. Clay Mineralogy. Clays Miner 37:29–40

Hazen RM (1976) Effects of temperature and pressure on the cell dimension and X-ray temperature factors of periclase T = 23 C, P = 1 atm, mounted on a cryo-tip with Be shroud. Am Mineral 61:266–271

Helland PE, Holmes MA (1997) Surface textural analysis of quartz sand grains from ODP Site 918 off the southeast coast of Greenland suggests glaciation of southern Greenland at 11 Ma. Palaeoclimatol Palaeoecol 135:109

Kesse GO (1985) The mineral and rock resources of Ghana. A.A. Balkema, Rotterdam/Boston, p 610

Kesse GO, Foster RP (1984) The occurrence of gold in Ghana, in Gold '82: The Geology, Geochemistry and Genesis of Gold Deposits. Rotterdam: Geological Society of Zimbabwe, A.A. Balkema, pp 648–650

Leube A, Hirdes W, Mauer R (1986) Project 80:2040

Lignie A, Granier D, Armand P, Haines J, Papet P (2012) Modulation of quartz-like GeO2 structure by Si substitution: an X-ray diffraction study of Ge1−xSixO2($0 \leq x < 0.2$) flux-grown single crystals. J Appl Cryst 45:272

Lin J-F, Vankó G, Jacobsen SD, Iota V, Struzhkin VV, Prakapenka VB, Kuznetsov A, Yo C-S (2007) Spin transition zone in earth's lower mantle. Science 317:1740

Lutterotti L (2010) Total pattern fitting for the combined size–strain–stress–texture determination in thin film diffraction. Nucl Inst Methods Phys Res B 268:334

Marquardt D (1963) An algorithm for least-squares estimation of nonlinear parameters. SIAM J Appl Math 11:431

McClenaghan MB (2005) Geochemical and pathfinder elements assessment in some mineralised regolith profiles in Bole-Nangodi gold belt in north-eastern Ghana. Expl Environ Anal 5:233

Nude PM, Asigri JM, Yidana SM, Arhin E, Foli G, Kutu JM (2012) Int J Geol 3:62

Nzulu G, Eklund P, Magnuson M (2021a) Characterization and identification of Au pathfinder minerals from an artisanal mine site using X-ray diffraction. J Mater Sci 56:7659

Nzulu GK, Bakhit B, Högberg H, Hultman L, Magnuson M (2021) Elucidating pathfinding elements for gold from the Alluvia small-scale mining site. Min 11:912–933

Plouffe A (2001) The glacial transport and physical partitioning of mercury and gold in till: implications for mineral exploration with examples from central British Columbia, Canada. Geol Soc Lond 185:287

Porter JK, McNaughton NJ, Evans NJ, McDonald BJ (2020) Rutile as a pathfinder for metals exploration. Ore Geol Rev 120:103406

Price JR, Bryan-Ricketts DS, Anderson D (2013) Weathering of Almandine garnet: influence of secondary minerals on the rate-determining step, and implications for regolith-scale Al mobilization. Clays Clay Miner 61:34

Smith SM, Amaor J (2014) Independent Technical report, NI 403-101, Kubi Gold project, Asante Gold Corporation, SEMS exploration

Somarin A, Zhou L, Steinhage I (2021) Application of handheld XRF on Ta-Nb-Sn-W ore: Factory calibration or user calibration? Geochem J 55:149